ORIGINAL ARTICLE

Journal Section

Spatial modeling of the membrane-cytosolic interface in protein kinase signal transduction

Wolfgang Giese[a] | Gregor Milicic[b] | Andreas Schröder[b] | Edda Klipp[a,1]

[a]Theoretische Biophysik, Humboldt-Universität zu Berlin, Berlin, Germany

[b]Department of Mathematics, University of Salzburg, Salzburg, Austria

[1]Corresponding author

Correspondence
Edda Klipp, Theoretical Biophysics, Humboldt-Universität zu Berlin, Berlin, 10115, Germany
Email: edda.klipp @ rz.hu-berlin.de

Funding information
This work was supported by a grant from the German Research Foundation (CRC 740 'From molecules to modules') to EK. GM and AS gratefully acknowledge support from the Sparkling Science research program of the Federal Ministry of Science, Research and Economy of Austria (BMWFW) within the Sparkling Science project "EMMA – Experimentation with mathematical algorithms" (SPA 05/172).

The spatial architecture of signaling pathways and the interaction with cell size and morphology are complex but little understood. With the advances of single cell imaging and single cell biology it becomes crucial to understand intracellular processes in time and space. Activation of cell surface receptors often triggers a signaling cascade including the activation of membrane-attached and cytosolic signaling components, which eventually transmit the signal to the cell nucleus. Signaling proteins can form steep gradients in the cytosol, which cause strong cell size dependence. We show that the kinetics at the membrane-cytosolic interface and the ratio of cell membrane area to the enclosed cytosolic volume change the behavior of signaling cascades significantly. We present a mathematical analysis of signal transduction in time and space by providing analytical solutions for different spatial arrangements of linear signaling cascades. These investigations are complemented by numerical simulations of non-linear cascades and asymmetric cell shapes.

KEYWORDS
signaling cascades | intracellular gradients | bulk-surface reaction-diffusion equations

Abbreviations: MAPK, mitogen-activated protein kinase; PC, pure cytosolic; MMC, mixed membrane-cytosolic; PDE, partial-differential equation.

1 | INTRODUCTION

Cells need to respond to a large variety of external stimuli such as environmental changes or extracellular communication signals. Signals transmitted from cell surface receptors to target genes in the nucleus are frequently transduced by cascades of covalent protein modifications. These modifications consist of inter-convertible protein forms, for instance, a phosphorylated and an unphosphorylated protein. Signaling cascades occur in many different variations including mitogen-activated protein-kinase (MAPK) cascades and small GTPase cascades.

Signal transduction mechanisms carried out by networks of protein-protein interactions are highly modular and regulatory behavior arises from relatively simple modifications Bhattacharyya et al. (2006). The spatial arrangement of signaling cascades varies in different biological systems. We focus on the localization of signaling components, which can be tethered to the cell-membrane or freely diffuse in the cytosol. Tethering to the cell-membrane can be mediated by protein prenylation Gelb et al. (2006); Wang and Casey (2016), co-localization by membrane-bound scaffolds Gordley et al. (2016) or membrane anchoring proteins Alberts et al.. Frequently, the first steps of signal transduction occur at the membrane and are then continued into the cytosol.

In many experimental and theoretical studies on signaling cascades, the cell is regarded as a number of well-mixed compartments with no variation in size, shape or organelle location. An extensive mathematical analysis of temporal aspects of signaling processes has been carried out in quantitative biology Heinrich et al. (2002); Kofahl and Klipp (2004); Klipp and Liebermeister (2006); Beguerisse-Díaz et al. (2016). However, the spatial description of signaling processes has received less attention despite its relevance in understanding cell morphology and growth regulation in time and space Kholodenko et al. (2010). Examples of spatial effects on the length scale of single cells range from the yeast mating process Maeder et al. (2007); Dudin et al. (2016) to the propagation of spatial information in hippocampal neurons which is controlled by cell shape and *vice versa* Neves et al. (2008); Chay et al. (2016).

We investigate linear signaling cascades with different realizations of spatial arrangements of signaling components as shown in Figure 1. Here, we focus on the membrane-cytosolic interface, which is included in the signaling motif shown in Figure 1(**B, C**).

Since the cytosol scales with cell volume and the cell membrane with the cell surface, reactions on the membrane and in the cytosol scale with the cell-surface to cell-volume ratio. For instance, we obtain an area/volume ratio of $\propto 3/R_{\mathrm{cell}}$ for a spherical cell geometry, where R_{cell} is the cell radius. We will show that this affects the global phosphorylation rate of signaling proteins that diffuse in the cytoplasmic volume, which depends on cell size. While cytosolic gradients naturally occur from the membrane to the nucleus, membrane-bound components can only form gradients along the membrane, which changes the response to heterogeneous signals. Furthermore, the diffusion on the membrane is much slower for membrane-bound components than for cytosolic components Klünder et al. (2013). Both of these factors are expected to largely change signal transduction properties of the pathway.

An analysis and comparison of spatial signal transduction motifs in response to spatially homogeneous and heterogeneous signals is presented in this study. The natural extension of widespread used ordinary differential equations are bulk-surface partial differential equations Elliott and Ranner (2012); Eigel and Müller (2017). Here, *bulk* refers to the cellular compartments that are represented as a volume such as the cytoplasm or the nucleus, while *surface* refers to all cellular structures that are represented as an area such as the cellular or nuclear membrane. Since their introduction to cell signaling systems Levine and Rappel (2005), bulk-surface partial differential equations have been successfully employed in several models for cell polarization Rätz and Röger (2012); Klünder et al. (2013); Giese et al. (2015); Thalmeier et al. (2016). However, membrane-cytosolic interfaces at different stages of a signaling cascade have not yet been investigated.

We start with an analysis of two different motifs with simplified linear kinetics, which allows to develop exact

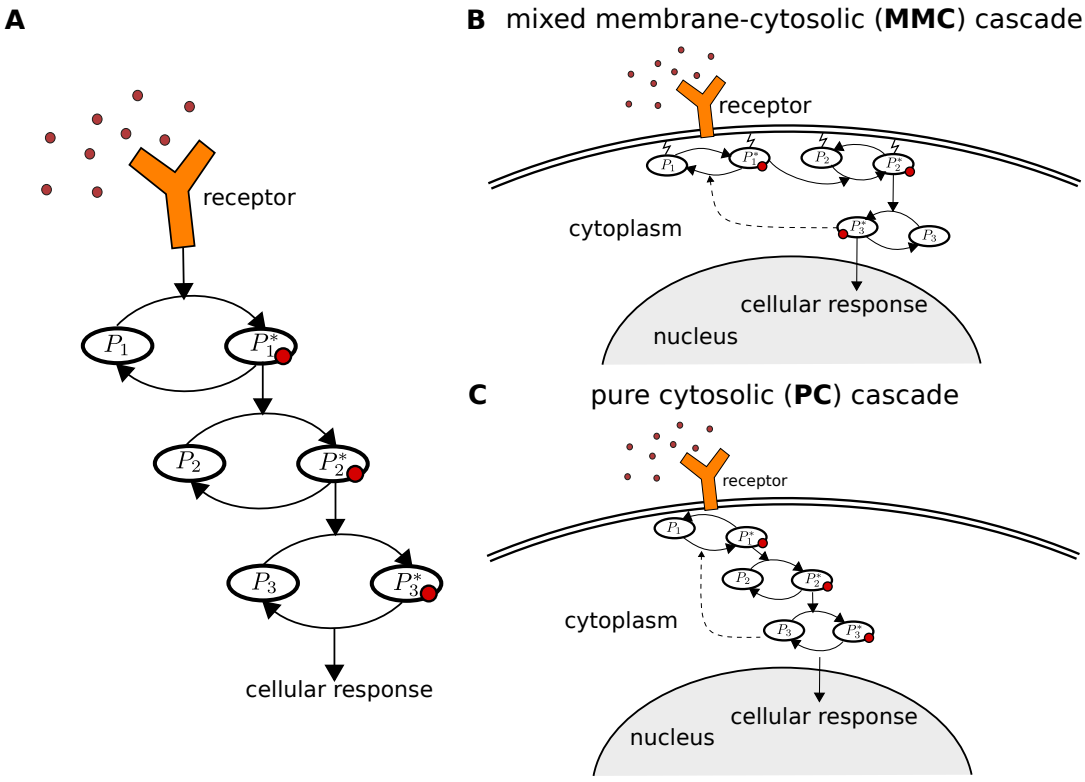

FIGURE 1 Spatial organization of signaling cascades. **A:** Sketch of the classical temporal signal transduction model. Extension of this model into three-dimensional space naturally results in a variety of different spatial motifs. **B:** The signal is first processed by signaling components tethered to the membrane, and then transduced at membrane-cytosolic interface into the cytosol. **C:** The signaling components are directly activated at the membrane-cytosolic interface and diffuse through the cytosol. Note, that diffusion coefficients for lateral diffusion along the membrane are much lower than in the cytosol.

analytical solutions of the steady state. Both motifs differ in their cell size dependence and we show further that their behavior can drastically differ from the assumption of well-mixed compartments. The time-scaling of signal transduction is investigated using the recently introduced method of local accumulation times Berezhkovskii et al. (2010). We continue by investigating the response and sensitivity to spatially heterogeneous signals such as signaling gradients for symmetrical and asymmetrical cell shapes. In the last section, we proceed with numerical investigations of systems with non-linear Hill kinetics as well as negative feedbacks and oscillations. A Fourier analysis in time is used to provide insight into the dependency of oscillation frequency and amplitude on cell size. Depending on the spatial motif, cell size limits for the extinction of oscillatory behavior are obtained.

2 | THE MODEL

We start with a linear signaling cascade with different localizations of the membrane-cytosolic interface as shown in Figure 1. We employ a simple cascade model from Heinrich et al. (2002), in which stimulation of a receptor leads to the

consecutive activation of several down-stream protein kinases. This model is extended into space in the following. We assume a linear cascade with N components, where the first $M < N$ components are localized at the membrane while the remaining $N - M$ components are assumed to freely diffuse in the cytosol. The equations for the membrane-bound components read

$$\frac{\partial P_n}{\partial t} = D_{\mathrm{mem}} \Delta_\Gamma P_n + v_n^a - v_n^d \qquad \text{on the cell membrane,}$$
$$\text{for} \quad n = 1, \ldots, M. \tag{1}$$

Here, $P_n(\vec{x}, t)$ are the local concentrations on the cell membrane and $P_0(\vec{x}, t)$ is the input signal. All of these species are functions of space and time, where $\vec{x}$ is a point on the membrane, t is the time and D_{mem} the diffusion rate on the cell membrane. Since the membrane is a surface in three-dimensional space with negligible thickness, the natural unit for concentrations of the cell membrane-bound species P_n, $n = 1, \ldots, M$ is molecules per area (see Table 2). The phosphorylation rates v_n^a as well as the dephosphorylation rates v_n^d have units molecules per area and time. Note, that if the input signal is homogeneous in space, meaning $P_0(\vec{x}, t) = P_0(t)$, all spatial fluxes $D_{\mathrm{mem}} \nabla_\Gamma P_k$ are zero and the equation system for the membrane-bound species can be described by an equivalent system of ordinary differential equations (SI text). In contrast to the membrane-bound signaling components $P_1, \ldots, P_M$, the signaling component P_{M+1} can freely diffuse in the cytosol. For the modeling of the membrane-cytosolic interface, we need to include diffusion in the cytosol and reactions on its boundaries, which are the membranes. These processes are modeled by a reaction-diffusion equation

$$\frac{\partial P_{M+1}}{\partial t} = D_{\mathrm{cyt}} \Delta P_{M+1} - v_{M+1}^d \qquad \text{in the cytosol,} \tag{2}$$

with the boundary condition

$$-D_{\mathrm{cyt}} \nabla P_{M+1} \cdot \vec{n} = v_{M+1}^a - v^i \qquad \text{on the cell membrane.} \tag{3}$$

Since P_{M+1} is activated by the upstream component P_M, which is tethered to the membrane, there is a phosphorylation reaction only on the cell membrane but not in the cytosol. This reaction is, therefore, modeled as a boundary condition. The reactions at the membrane-cytosolic interface are described by the phosphorylation rate v_{M+1}^a and the dephosphorylation rate v^i, both with units molecules per area and time. The species P_{M+1} diffuses freely in the cytosolic volume with the diffusion rate D_{cyt} and therefore its local concentration is described in molecules per volume. The dephosphorylation rate v_{M+1}^d is, therefore, given in molecules per volume and time. For the flux on all other membrane enclosed organelles we assume a zero-flux condition

$$-D_{\mathrm{cyt}} \nabla P_{M+1} \cdot \vec{n} = 0. \tag{4}$$

The equations for the components of the downstream cytosolic cascade read

$$\frac{\partial P_n}{\partial t} = D_{\mathrm{cyt}} \Delta P_n + v_n^a - v_n^d, \qquad \text{in the cytosol,}$$
$$\text{for} \quad n = M + 2, \ldots, N. \tag{5}$$

The concentrations at position $\vec{x}$ in the cytosolic volume at time t of the cytosolic components, $P_n(\vec{x}, t)$ with $n = M + 1, \ldots, N$, are given in molecules per volume (see Table 2). For the cytosolic components we assume zero-flux conditions:

$$-D_{\mathrm{cyt}} \nabla P_n \cdot \vec{n} = 0, \qquad \text{on the cell membrane,} \tag{6}$$

$$-D_{\mathrm{cyt}} \nabla P_n \cdot \vec{n} = 0, \qquad \text{on the nuclear membrane,} \tag{7}$$

$$\text{for} \quad n = M + 2, \ldots, N.$$

In classical MAPK cascades the last component of the cascade, which is the phosphorylated MAPK is imported into the nucleus. Examples range from Hog1 nuclear import in yeast Klipp et al. (2005); Muzzey et al. (2009) to the import of ERK in mammals Nardozzi et al. (2010). In this case the boundary condition (7) on the nucleus for the last cytosolic component P_N needs to be modified to

$$-D_{\mathrm{cyt}} \nabla P_N \cdot \vec{n} = -\epsilon P_N, \tag{8}$$

where ϵ represents a nuclear-import reaction rate on the nuclear membrane.

We will test and compare systems with three components $N = 3$ as shown in Figure 1, where the spatial arrangement of the components is varied. Here, $M = 2$ describes the case of two membrane-bound and one cytosolic element (motif Figure 1**B**) and $M = 0$ the case of only cytosolic components (motif Figure 1**C**). In the following the case $M = 2$ is referred to as mixed membrane-cytosolic (MMC) and $M = 0$ as pure cytosolic (PC) cascade.

3 | RESULTS

3.1 | The mixed membrane-cytosolic cascade is strongly size dependent

A spherical cell with radius R_{cell} is assumed in the following analysis. The nucleus is as well represented as sphere with radius R_{nuc}, which is placed at the center of the cell. The input signal is denoted by $P_0(t)$ and is assumed to be homogeneous on the cell surface. The concentrations of protein kinases are described by functions $P_i(r, t)$ depending on space and time. Note, since the cellular geometry is radially symmetric and the input signal P_0 acts homogeneously on the cell membrane, these functions depend only on the radial distance from the origin denoted by r and time t. The model equations for the mixed membrane-cytosolic cascade (MMC, $M = 2$) with linearized kinetics read

$$\frac{\partial P_1}{\partial t} = D_{\mathrm{mem}} \Delta_\Gamma P_1 + \alpha_1 P_0 - \beta_1 P_1 \qquad \text{on the membrane,} \tag{9}$$

$$\frac{\partial P_2}{\partial t} = D_{\mathrm{mem}} \Delta_\Gamma P_2 + \alpha_2 P_1 - \beta_2 P_2 \qquad \text{on the membrane,} \tag{10}$$

$$\frac{\partial P_3}{\partial t} = D_{\mathrm{cyt}} \Delta P_3 - \beta_3 P_3 \qquad \text{in the cytosol,} \tag{11}$$

and boundary conditions for the cytosolic species P_3:

$$-D_{\mathrm{cyt}} \nabla P_3 \cdot \vec{n} = \alpha_3 P_2 - \gamma P_3 \qquad \text{on the membrane,} \tag{12}$$

$$-D_{\mathrm{cyt}} \nabla P_3 \cdot \vec{n} = -\epsilon P_3 \qquad \text{at the nucleus.} \tag{13}$$

Here, α_i describe phosphorylation and β_i desphosphorylation rates. In (11), the rate γ with units $\mu m/s$ describes saturation of the activation reaction on the membrane.

The steady state for the first two elements is given by $\bar{P}_1 = \frac{\alpha_1}{\beta 1} P_0$ and $\bar{P}_2 = \frac{\alpha_1 \alpha_2}{\beta 1 \beta_2} P_0$. For the steady state of P_3, the solution is given by

$$\bar{P}_3(r) = A i_0\left(r\sqrt{\frac{\beta_3}{D_{\mathrm{cyt}}}}\right) + B k_0\left(r\sqrt{\frac{\beta_3}{D_{\mathrm{cyt}}}}\right), \tag{14}$$

where the coefficients A and B are derived in the SI text. The steady state solution for different cell sizes is shown in Figure 2. The concentration is maximal at the cell membrane and decays towards the nucleus. An approximation of the decay length L_{gradient} of the intracellular gradient (with highest concentration at the membrane) is given by Brown and Kholodenko (1999)

$$L_{\mathrm{gradient}} = \sqrt{\frac{D_{\mathrm{cyt}}}{\beta_3}}. \tag{15}$$

This decay length can be compared with the actual cell size. Their ratio is called the Thiele modulus, a dimensionless measure defined as $\Phi = \frac{R_{\mathrm{cell}}}{L_{\mathrm{gradient}}} = \sqrt{\frac{\beta_3 R_{\mathrm{cell}}^2}{D_{\mathrm{cyt}}}}$ Meyers et al. (2006). For $\Phi > 1$ strong intracellular gradients and concentration heterogeneities of signaling molecules are to be expected, while for $\Phi < 1$ the concentration is almost homogeneous.

The effect of cell size on intracellular concentration gradients is shown in Figure 2. However, the cell size dependence in cell signaling systems does not only arise by the characteristic length scale for intracellular gradient formation L_{gradient} as reported in Brown and Kholodenko (1999); Meyers et al. (2006), but by the change of absolute intracellular concentration levels. The dependence of absolute concentration levels on the membrane-cytosolic interface is shown in Figure 2 and supplementary Figure S1 for a set of different parameters.

In the special case that there is no nucleus or excluding volume, $R_{\mathrm{nuc}} = 0$, we have $B = 0$ and the steady state solution reads

$$\begin{aligned} \bar{P}_3(r) &= A i_0\left(r\sqrt{\frac{\beta_3}{D_{\mathrm{cyt}}}}\right), \\ A &= \frac{\alpha_3 P_2}{\sqrt{D_{\mathrm{cyt}}\beta_3}\, i_1\left(R_{\mathrm{cell}}\sqrt{\frac{\beta_3}{D_{\mathrm{cyt}}}}\right) + \gamma i_0\left(R_{\mathrm{cell}}\sqrt{\frac{\beta_3}{D_{\mathrm{cyt}}}}\right)}. \end{aligned} \tag{16}$$

The coefficient A represents the minimal concentration in the cell center ($r = 0$). The maximal concentration at the cell membrane is bounded by

$$\frac{\alpha_3 P_2}{\sqrt{D_{\mathrm{cyt}}\beta_3} + \gamma} < P_3(R_{\mathrm{cell}}) < \frac{\alpha_3 P_2}{\gamma}. \tag{17}$$

The concentration level at the membrane tends towards the upper bound in the limit of small cells, meaning $\Phi \ll 1$, while it tends towards the lower bound in the limit of large cells, meaning $\Phi \gg 1$. This effect is shown in supplementary Figure S1. Note, that for a large inactivation rate at the membrane-cytosolic interface $\gamma > \sqrt{D_{\mathrm{cyt}}\beta_3}$, the cell size dependence decreases. Therefore, cell size dependence is mainly determined by γ and $\sqrt{D_{\mathrm{cyt}}\beta_3}$ but is independent of the phosphorylation rate α. In order to achieve cell size independence and a reasonable concentration of phosphorylated

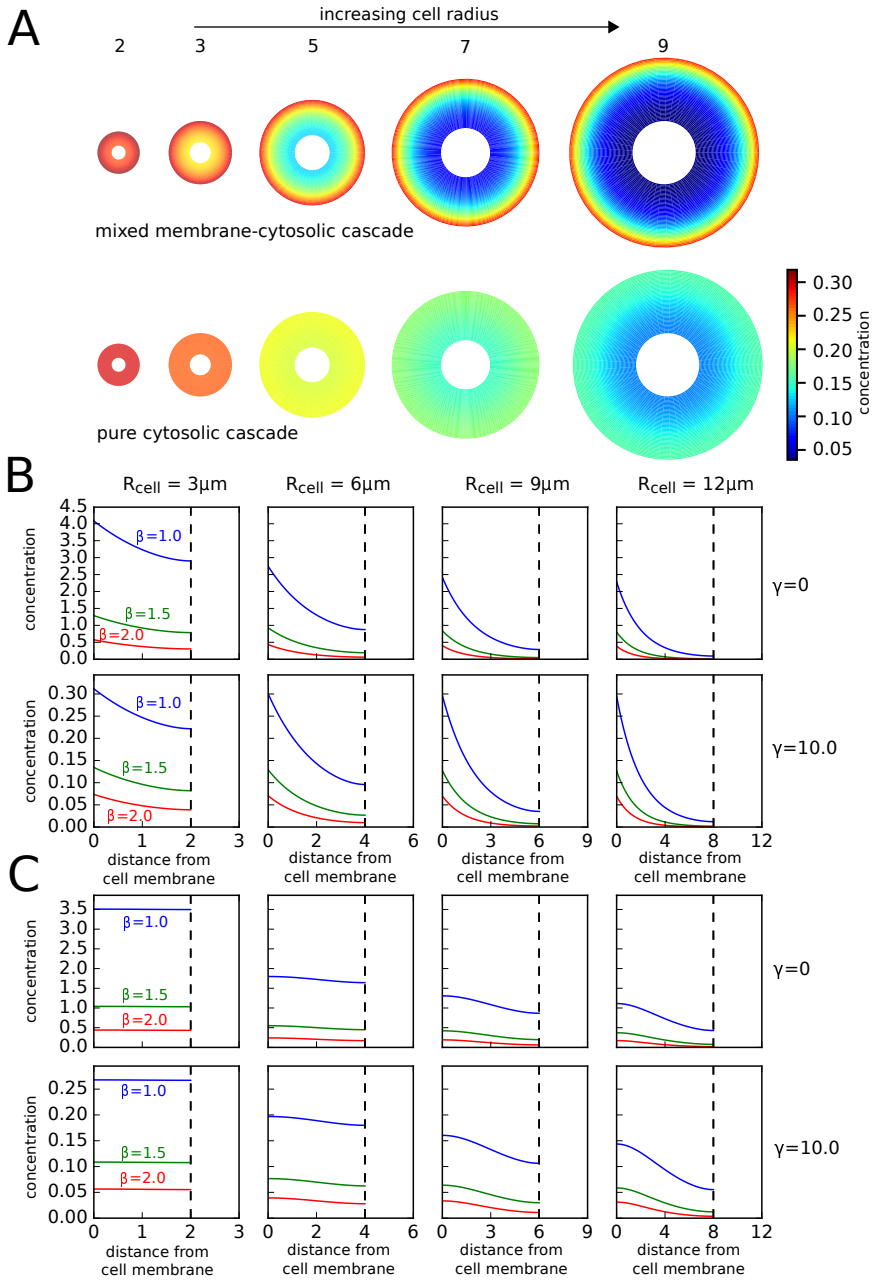

FIGURE 2 Intracellular concentration profiles for two different signal-transduction motifs. **A:** The concentration of the third cascade element P_3 was plotted along a slices through three-dimensional cells. The numbers below the cells indicate the cell radius in microns, the radius of the nucleus is 1/3 of the cell radius. Strong intracellular concentration gradients are generated in the case of the MMC cascade with two membrane-bound components and only one cytosolic species [above]. Concentration gradients are much shallower for the pure cytosolic cascade, where all three components diffuse freely in the cytosol [below]. The parameters used were $D_{\mathrm{mem}} = 0.03$, $D_{\mathrm{cyt}} = 3.0$, $\alpha_1 = \alpha_2 = \alpha_3 = 1.5$, $\beta_1 = \beta_2 = \beta_3 = 1.0$, $\gamma = 10.0$, $P_0 \equiv 1.0$. **B:** A MMC cascade with two membrane-bound components and only one cytosolic species is shown. **C:** In contrast the PC cascade, where all three components diffuse freely in the cytosol exhibits much shallower gradients. For both spatial motifs size dependence of the concentration level decreases with higher values of γ.

signaling molecules, the phosphorylation rate α has to be increased together with γ.

We can further investigate the evolution of the average concentration levels for this model in the case $\gamma = 0$, which implies strong cell size dependence. In case of arbitrary cell shapes with cell volume V_{cell} and cell membrane area M_{cell}, the average concentration level is obtained from

$$P_3^{\mathrm{avg}} = \frac{1}{|V_{\mathrm{cell}}|} \int_{V_{\mathrm{cell}}} P_3 \, dV. \tag{18}$$

It can be shown that in this case the average concentration levels follow the system of ordinary differential equations

$$\frac{dP_1^{\mathrm{avg}}(t)}{dt} = \alpha_1 P_0^{\mathrm{avg}}(t) - \beta_1 P_1^{\mathrm{avg}}(t), \tag{19}$$

$$\frac{dP_2^{\mathrm{avg}}(t)}{dt} = \alpha_2 P_1^{\mathrm{avg}}(t) - \beta_2 P_2^{\mathrm{avg}}(t), \tag{20}$$

$$\frac{dP_3^{\mathrm{avg}}(t)}{dt} = \frac{|M_{\mathrm{cell}}|}{|V_{\mathrm{cell}}|} \alpha_3 P_2^{\mathrm{avg}}(t) - \beta_3 P_3^{\mathrm{avg}}(t), \tag{21}$$

where P_1^{avg} and P_2^{avg} are the average concentration levels in molecules per cell membrane area. For a derivation see supplementary text S1. The steady state for the average concentration of P_3 is given by

$$\bar{P}_3^{\mathrm{avg}} = \frac{|M_{\mathrm{cell}}|}{|V_{\mathrm{cell}}|} \frac{\alpha_1 \alpha_2 \alpha_3 P_0}{\beta_3}. \tag{22}$$

Therefore, the average concentration level scales with the ratio of $\frac{|M_{\mathrm{cell}}|}{|V_{\mathrm{cell}}|}$. The effective global phosphorylation rate for the average concentration of active signaling molecules in the cytosol is therefore determined by $\tilde{\alpha}_3 = \frac{|M_{\mathrm{cell}}|}{|V_{\mathrm{cell}}|} \alpha_3$. These relations give us a correspondence between widespread used ordinary differential equations and the bulk-surface partial differential equations employed in this paper. In summary, we have strong cell size dependence, with decreasing concentrations for larger cells. For cells with $\Phi > 1$ also the concentration differences from cell membrane to cell nucleus become important and a description in terms of average concentration may become invalid.

3.2 | Efficient cytosolic transport via cytosolic cascades

In the following we consider a PC (pure cytosolic) cascade with three elements, in which all elements freely diffuse through the cytosol. The reaction-diffusion system is given by

$$\frac{\partial P_1}{\partial t} = D_{\mathrm{cyt}} \Delta P_1 - \beta_1 P_1, \tag{23}$$

$$-D_{\mathrm{cyt}} \nabla P_1 \cdot \vec{n} = \alpha_1 S_R - \gamma_1 P_1, \tag{24}$$

$$\frac{\partial P_2}{\partial t} = D_{\mathrm{cyt}} \Delta P_2 + \alpha_2 P_1 - \beta_2 P_2, \tag{25}$$

$$-D_{\mathrm{cyt}} \nabla P_2 \cdot \vec{n} = 0, \tag{26}$$

$$\frac{\partial P_2}{\partial t} = D_{\mathrm{cyt}} \Delta P_3 + \alpha_3 P_2 - \beta_3 P_3, \tag{27}$$

$$-D_{\mathrm{cyt}} \nabla P_3 \cdot \vec{n} = -\epsilon P_3. \tag{28}$$

In the special case of $\beta_1 = \beta_2 = \beta_3 = \beta$ analytical approximations to cytosolic cascades in a one-dimensional system have been derived in Stelling and Kholodenko (2009); Muñoz-García et al. (2009). While a one-dimensional cellular geometry can be used to study gradient formation qualitatively, spatial effects such as the cell surface to volume ratio are neglected. Therefore, we present exact analytical solutions to the linear system in three dimensions. The steady state solutions for $\bar{P}_n(r)$ are expanded as follows

$$\bar{P}_n(r) = \sum_{k=1}^{n} A_{n,k} r^{k-2} \exp(\sqrt{\frac{\beta}{D}} r) + \sum_{k=1}^{n} B_{n,k} r^{k-2} \exp(-\sqrt{\frac{\beta}{D}} r). \tag{29}$$

The algebraic expressions of the coefficients $A_{n,k}$ and $B_{n,k}$ and their derivation are shown in the SI text. In comparison to the MMC cascade, which was discussed in the previous section, the third cascade element P_3 is more evenly distributed in the cell and concentration gradients are much more shallow (see Figure 2). In the case $\gamma = 0$, we can derive a expressions for the steady states of the average concentration of signaling components, which are given by

$$\bar{P}_1^{\text{avg}} = \frac{|M_{\text{cell}}|}{|V_{\text{cell}}|} \frac{\alpha_1}{\beta} P_0, \qquad \bar{P}_2^{\text{avg}} = \frac{|M_{\text{cell}}|}{|V_{\text{cell}}|} \frac{\alpha_1 \alpha_2}{\beta} P_0,$$
$$\bar{P}_3^{\text{avg}} = \frac{|M_{\text{cell}}|}{|V_{\text{cell}}|} \frac{\alpha_1 \alpha_2 \alpha_3}{\beta} P_0. \tag{30}$$

Therefore, the average concentration of the third cascade element P_3^{avg} takes the same values in the MMC and PC cascade. The major distinction of both spatial motifs is given by the fact that the concentration differences obtained at the cell membrane and nucleus are larger in the MMC cascade than in the PC cascade. Similarly as in the previous section, we can formulate a system of ordinary differential equations for the average concentrations

$$\frac{dP_1^{\text{avg}}(t)}{dt} = \frac{|M_{\text{cell}}|}{|V_{\text{cell}}|} \alpha_1 P_0^{\text{avg}}(t) - \beta_1 P_1^{\text{avg}}(t), \tag{31}$$
$$\frac{dP_2^{\text{avg}}(t)}{dt} = \alpha_2 P_1^{\text{avg}}(t) - \beta_2 P_2^{\text{avg}}(t), \tag{32}$$
$$\frac{dP_3^{\text{avg}}(t)}{dt} = \alpha_3 P_2^{\text{avg}}(t) - \beta_3 P_3^{\text{avg}}(t). \tag{33}$$

The dependence of absolute concentration levels on the membrane-cytosolic interface is shown in Figure 2 and supplementary Figure S1 for a set of different parameters.

3.3 | The timing of spatial signaling

The timing of signal transduction in linear signaling cascades for well-stirred homogeneous systems has been analyzed in Heinrich et al. (2002). It was shown that phosphatases have a more pronounced effect than kinases on the rate and duration of signaling, whereas signal amplitude is controlled primarily by kinases. A thorough analysis of linear models assuming a homogeneous distribution of signaling molecules for different kinds of external stimuli has been recently worked out in Beguerisse-Díaz et al. (2016). Here, we want to extend and compare these findings to spatial signal transduction omitting the simplification of homogeneous concentrations. The time-scale analysis for spatial models is more difficult and therefore we used the recently introduced measure of accumulation times Berezhkovskii et al. (2010).

TABLE 1 An overview on values and parameters. The numerical values given in the paper all use the units shown in this table.

entity	value	unit	description
D_{mem}	3.0×10^{-2}	$\mu m^2/s$	diffusion coefficient for the membrane-bound species
D_{cyt}	3.0	$\mu m^2/s$	diffusion coefficient for the cytosolic species
α_i	-	s^{-1}	phosphorylation rate
β_i	-	s^{-1}	phosphatase activity
γ	-	$\mu m/s$	reaction rate at the membrane- cytosolic interface
			at the cell membrane
ϵ	-	$\mu m/s$	import rate/permeability at the membrane- cytosolic interface at the nucleus
$R_{\mathrm{cell}}, R_{\mathrm{nuc}}$	-	μm	radius of the cell/nucleus

TABLE 2 An overview on values and parameters. The numerical values given in the paper all use the units shown in this table.

The fraction of this steady state level that accumulated at distance r and time t is expressed as

$$\rho(r,t) = (\bar{P}_i(r) - P(r,t))/\bar{P}_i(r). \tag{34}$$

The difference $\rho(r,t_1) - \rho(r,t_2)$ can be interpreted as the fraction of the steady state level $\bar{P}_i(r)$ that accumulated in the time interval $[t_1, t_2]$. In an infinitesimal time interval $[t, t+dt]$ the fraction of accumulated activated signaling molecules at steady state is given by $-\frac{\partial\rho(r,t)}{\partial t}dt$. Note, that $\frac{\partial\rho(\vec{x},t)}{\partial t}$ satisfies

$$\int_0^\infty \frac{\partial\rho(r,t)}{\partial t}dt = 1, \tag{35}$$

since the initial condition at time $t = 0$ is given by $P_n(r,0) \equiv 0$. Based on this expression the local accumulation time is defined as Berezhkovskii et al. (2010)

$$\tau(r) = -\int_0^\infty t\frac{\partial\rho(r,t)}{\partial t}dt.$$

The accumulation time can be derived from the steady state solution even if no closed form of the time-dependent solution is known Berezhkovskii et al. (2010). The timing of the average concentrations given in the system of ordinary differential equations for the MMC cascade (19) - (21) and the PC cascade (31) - (33) are the same and can be analytically expressed as

$$\tau(r) = \frac{1}{\beta_1} + \frac{1}{\beta_2} + \frac{1}{\beta_3}. \tag{36}$$

This expression also coincides with signaling times calculated by Heinrich et al. Heinrich et al. (2002). However, for the spatial model the local accumulation times at the membrane and nucleus differ. They are generally faster at the membrane and slower at the nucleus, where the degree of the difference increases with cell size (see Figure 3). Furthermore, also the two spatial motifs show significant differences. For the MMC cascade the accumulation time for the second element P_2 is exactly $\frac{1}{\beta_1} + \frac{1}{\beta_2}$ on the membrane, while it is faster for the cytosolic species (compare Figure 3). The accumulation time of P_3 at the nucleus is, as expected, much longer. For a small cell with a Thiele modulus of $\Phi < 1$, the intracellular concentration is spatially homogeneous and the approximation $\frac{1}{\beta_1} + \frac{1}{\beta_2} + \frac{1}{\beta_3}$ holds, while for signal propagation to the nucleus increases with cell size. An analytical solution of the accumulation times for P_3 for the MMC cascade and the special case of $R_{\mathrm{nuc}} = 0$ can be derived Ellery et al. (2013), which is given in the SI Text. The accumulation time for the signal at the nucleus is, as expected longer. For a small cell with $\Phi < 1$, the intracellular concentration is spatially almost homogeneous and again the approximation $\frac{1}{\beta_1} + \frac{1}{\beta_2} + \frac{1}{\beta_3}$ holds. However, for larger cells, the time for signal propagation to the nucleus increases with cell size. For the PC cascade, the increase in accumulation time at the nucleus with cell size is less pronounced than for the mixed-membrane cytosolic cascade.

While a constant stimulus was applied to calculate the accumulation times, we also tested a decaying signal $P_0(t) = \exp(-\lambda t)$. A comparison of the MMC and PC is shown in Figure 3. Interestingly, the concentration level at the membrane for the PC cascade decreases from the first level P_1 to the second level P_2 and than increases again from the second P_2 to the third P_3 level, while there is an increase from cascade level to cascade level at the nucleus. This phenomenon is caused by the concentration differences from cell membrane to nucleus, which is larger for P_1 than for P_2 in the PC cascade. Note, that the parameters were chosen as $\frac{\alpha}{\beta} = 2$), which means a twofold increase for the average concentration levels from one signaling cascade element to the next. Therefore, the spatial system can behave entirely different than the homogeneous system.

For calculation of higher moments of the time scaling and the special case of a cell without nucleus we refer to Ellery et al. (2013). An analysis for time scaling of a linear cascade in one spatial dimension with four elements including higher moments has been carried out in Simpson et al. (2013).

3.4 | Quantifying the pathway sensitivity with respect to spatially heterogeneous signals

In the following we present a method for analyzing the signal transduction of heterogeneous signals. The signaling cascade can be spatially localized as in the case of directed growth. Examples are *S. cerevisie* Maeder et al. (2007) or *S. pombe* Dudin et al. (2016). Biochemical properties of protein-protein interactions and morphological properties can be tightly connected Peletier et al. (2003). We test the linear signaling cascade with a graded stimulus of the form

$$P_0(\vec{x}) = P_0^{\mathrm{base}} + P_0^{\mathrm{slope}}(x_1 - x_1^{\mathrm{mid}}), \qquad \vec{x} = (x_1, x_2, x_3), \tag{37}$$

where P_0^{Base} and P_0^{slope} are constants describing the basal signal strength and the slope of the signal, respectively. Here we choose the origin coordinates to be in the center of the cell and, therefore, $x_1^{\mathrm{mid}} = 0$.

The gradient can naturally be defined as the difference of concentration at two points over the euclidean distance of these two points. In the case of the kinase concentrations, the gradient can be computed from $(P_n(\vec{x}_{\mathrm{front}}) - P_n(\vec{x}_{\mathrm{back}}))/|\vec{x}_{\mathrm{front}} - \vec{x}_{\mathrm{back}}|$. However, to compare gradients of kinases at different levels, we calculated a normalized

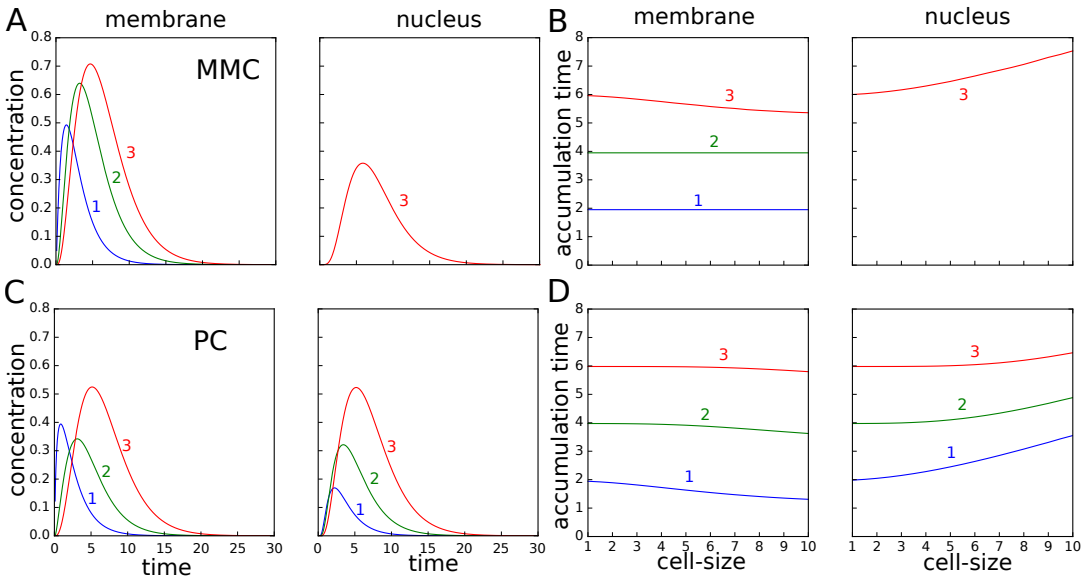

FIGURE 3 Signaling time at the membrane and nucleus for the mixed membrane-cytosolic (MMC) cascade (**A,B**) and pure cytosolic (PC) cascade (**C,D**) at the membrane and at the nucleus. **A**: Time course of the concentration of P_1, P_2 and P_3 for the mixed membrane-cytosolic cascade. The cascade levels are indicated by the numbers. The signal $P_0(\vec{x}, t) = \exp(-\lambda t)$ was applied and the parameters used were $R_{\text{cell}} = 6\mu m$, $R_{\text{nuc}} = 2\mu m$, $\lambda = 1$, $\alpha_1, \alpha_2, \alpha_3 = 1$ and $\beta_1, \beta_2, \beta_3 = 0.5$. **B**: Simulation of the pure cytosolic cascade, but otherwise the same setup and parameters as in (**A**). **C**: Accumulation times for the mixed membrane-cytosolic cascade. In this scenario, a constant signal $P_0(\vec{x}, t) = 1$ was applied and the cells size varied. The ratio of cellular to nuclear radius was kept at $R_{\text{cell}}/R_{\text{nuc}} = 3$. Otherwise the same parameters as in (**A**) and (**B**) were used. **D**: Simulation of the pure cytosolic cascade, but with the same setup and parameters as in (**C**),

gradient in order to eliminate signal amplification of the total concentration

$$\text{grad}^{\text{norm}}_{\text{cell}} P_n = \frac{1}{P_n^{\text{cell}}} \frac{P_n(\vec{x}_{\text{front}}) - P_n(\vec{x}_{\text{back}})}{|\vec{x}_{\text{front}} - \vec{x}_{\text{back}}|}, \tag{38}$$

$$\text{grad}^{\text{norm}}_{\text{nuc}} P_n = \frac{1}{P_n^{\text{nuc}}} \frac{P_n(\vec{x}_{\text{front}}) - P_n(\vec{x}_{\text{back}})}{|\vec{x}_{\text{front}} - \vec{x}_{\text{back}}|}, \tag{39}$$

where P_n^{cell} and P_n^{nuc} are the average concentrations on the cell membrane and at the nucleus, respectively. For both spatial motifs we performed a parameter study (see Figure 4).

Interestingly, the gradient of the third cascade level P_3 first increases and than decreases for both spatial motifs. This effect is much more pronounced at the nucleus than at the membrane. It can be explained by the effect that for a small cells, the concentration is almost homogeneous in the cytosol and concentration differences are balanced by diffusion. However, with increasing cell size the absolute concentration level decreases in the cell and at the nucleus. As a consequence, also the absolute gradient decreases. The normalized gradient at the nucleus for the PC cascade behaves qualitatively similar for the MMC cascade, however the peak for the normalized gradient is obtained for larger cell sizes. For the PC cascade the normalized gradient is increasing with cell size in the observed range of cell sizes.

The findings can also be generalized to higher order spatial heterogeneities, meaning heterogeneities with multiple

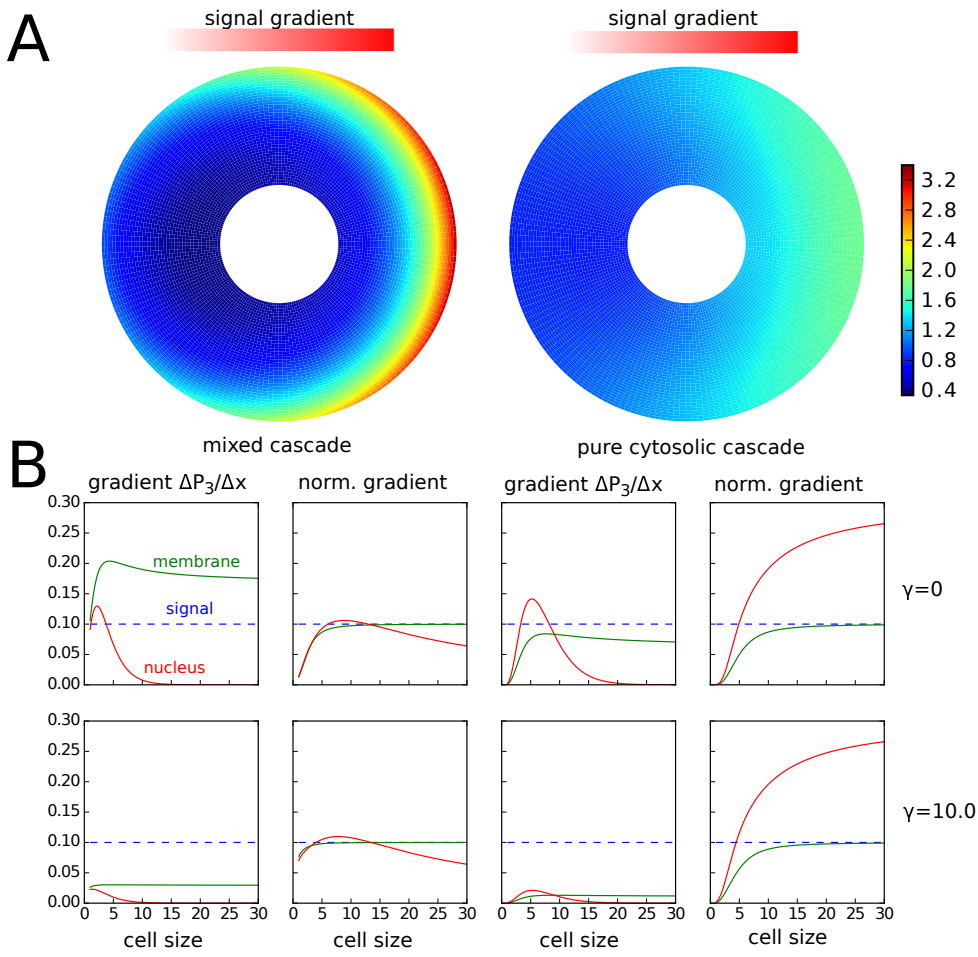

FIGURE 4 Intracellular concentration profile in response to a linear gradient. The mixed membrane-cytosolic (MMC) cascade with two membrane-bound components and only one cytosolic species exhibits a much stronger response [left] than the the pure cytosolic (PC) cascade, where all three components diffuse freely in the cytosol. Interestingly, for the gradient that is sensed at the cell surface can be higher than the gradient of the signal, which is due to the barrier that the nucleus causes. For the pure cytosolic model theses accumulation effects are most pronounced for the gradient at the nucleus. For both spatial motifs the spatial response to the gradient decreases with higher values of γ. The parameters used were $\alpha_1 = \alpha_2 = \alpha_3 = 2.0$, $\beta_1 = \beta_2 = \beta_3 = 1.5$, $P_0^{\text{base}} = 1.0$ and $P_0^{\text{slope}} = 0.1$.

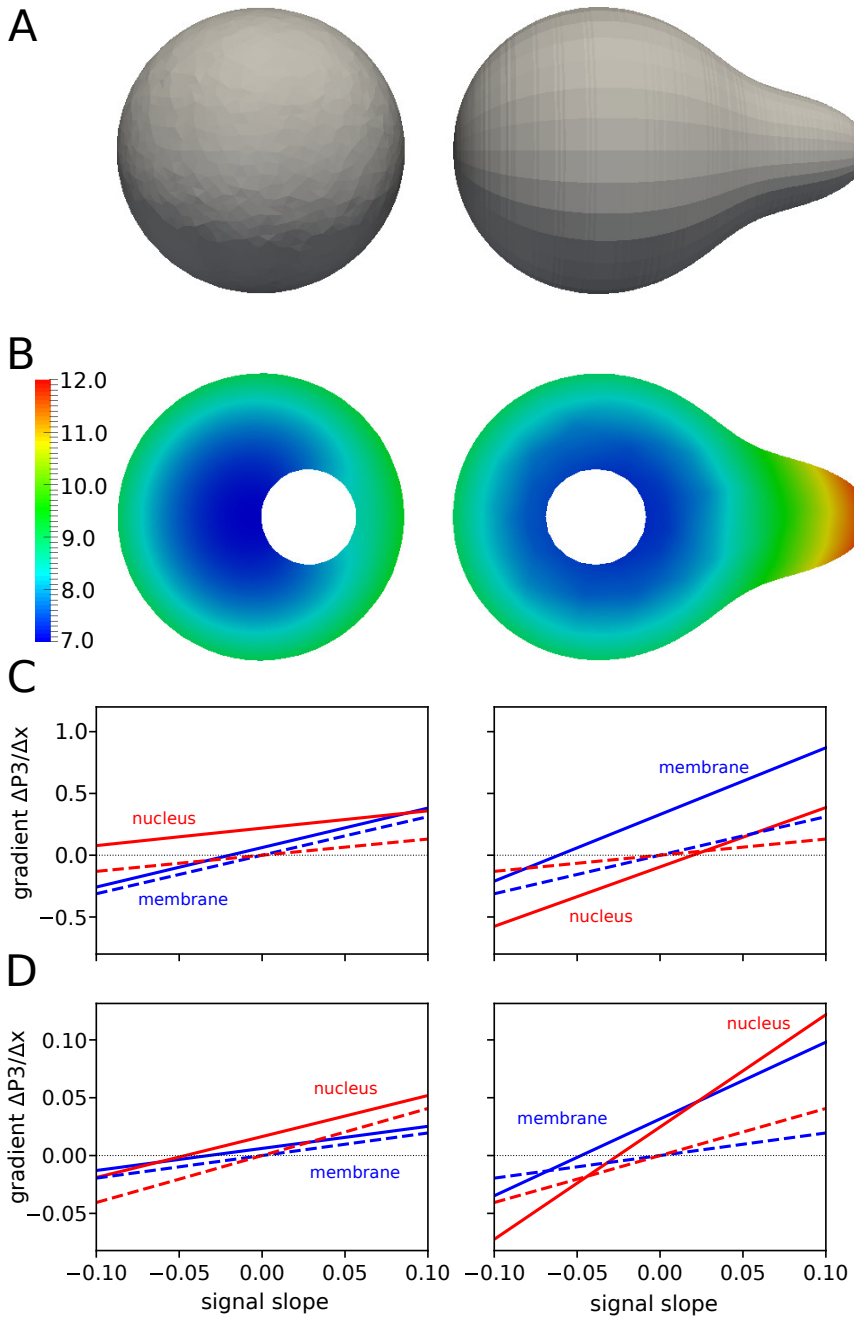

FIGURE 5 Response of the two cascade systems (MMC and PC) for different cellular asymmetries to a linear gradients with varying slope P_0^{slope}. **A** and **B**: The two investigated cell shapes. A spherical cell with $R_{\text{cell}} = 3\,\mu m$, $R_{\text{nuc}} = 1\,\mu m$ and a nucleus shifted to the side as well as a cell with a protrusion. **B**: Profile of P_3 after stimulation with a spatially homogeneous signal , meaning $P_0^{\text{slope}} = 0.0$. Due to the cellular asymmetry in organelle position (left) and asymmetric cell shape (right) a gradient along the cell membrane and nuclear membrane is generated, which would not be generated for a symmetric cell. **C**: Response to different values of P_0^{slope} for the MMC cascade. The response of a symmetric cell with $R_{\text{cell}} = 3\,\mu m$ and $R_{\text{nuc}} = 1\,\mu m$ is indicated with dashed lines for comparison. The gradient of P_3 in case of the cellular asymmetry is altered (solid lines). **D**: Same setup for the PC cascade. The parameters used were $\alpha_1 = \alpha_2 = \alpha_3 = 1.0, \beta_1 = \beta_2 = \beta_3 = 0.5, \gamma = 0.0$ and $P_0^{\text{base}} = 1.0$.

maxima and minima (see SI Text). The signal can be decomposed using spherical harmonics

$$P_0(\theta, \phi, t) = \sum_{l=0}^{\infty} \sum_{m=-l}^{l} A_{0,l}^m(t) Y_l^m(\theta, \phi), \tag{40}$$

$$A_{0,l}^m(t) = \int_0^{2\pi} \int_0^{\pi} P_0(\theta, \phi, t) Y_l^{m*}(\theta, \phi) \sin(\theta)\, d\theta d\phi. \tag{41}$$

In this decomposition the amplitudes of higher order, where the order is denoted by l, are generally more strongly damped than gradients or spatial heterogeneities of lower order (see SI Text). In this manner, the results shown here can be extended to complex spatial signals on the cell surface.

Furthermore, we tested the influence of asymmetries in cell shape and organelle position. The first asymmetry is a cell with a nucleus moved away from the cell center (see Figure 5). The second asymmetry is a cell with a protrusion, as occurs for instance in mating yeast Diener et al. (2014). Both cellular asymmetries induce an intracellular gradient along the cell membrane as well as the nuclear membrane even if a spatially homogeneous gradient is applied on the cell surface (see Figure 5**B**). For a cell with the nucleus moved away from the center a gradient is induced, since the nucleus acts like a dam against the diffusive flux from the membrane into the cytosol (see Figure 5**B**). For the cell with a protrusion the concentration of P_3 is higher in the protrusion than in the opposite distal end, which is the spherical part of the cell. This effect emerges due a higher local surface to volume ratio in the protrusion region. Therefore, a larger portion of cytosolic signaling molecules, which freely diffuse in the cytosol, is phosphorylated in the protrusion part leading to a gradient from the protrusion tip to the opposite distal end of the cell. The influence of cellular asymmetries has also been investigated in Giese et al. (2015) for gradients of the small Rho-GTPase Cdc42 during cell polarization. However, this system reacts in the opposite way since the flux of molecules is directed from the cytosol onto the membrane and one observes a gradient of from the distal end to the protrusion. For a cell with an organelle moved away from the cell center, the polarization system results in a lower concentration in the vicinity of the organelle. These effects occur due to the different architectures of both systems. In the PC and MMC signaling cascades, we have signal transduction from the membrane to the nucleus and, therefore, a diffusive flux of activated signaling molecules from the membrane into the cytosol, while in the polarization system the flux of signaling molecules is directed from the cytosol onto the membrane, which is the opposite direction. Therefore, both system respond differently to cellular asymmetries with respect to gradient formation. This interplay of both systems is especially interesting, since in many organisms a polarization system is interacting with a MAPK cascade Thomson et al. (2011); Ventura et al. (2014). To complete our investigations, we varied the slope of the signal and investigated the sensitivity of both cell shapes towards different slopes of signals and compared the response with a symmetric cell (see Figure 5**C**).

4 | DISCUSSION

Stimulated by the progress in cell imaging and the increasing need to understand intracellular dynamics, we investigated and discussed a general approach of modeling cellular signal transduction in time and space. We showed that modeling of the membrane-cytosolic interface is crucial as well as the ratio of membrane area and cytosolic volume, which are both spatial properties. The results imply strong cell size dependence of signal transduction within cells. Widely used time-dependent models of ordinary differential equations can naturally be extended into space by using bulk-surface differential equations. Applying this extension to a class of linear signal transduction models, we compared the assumption of a well mixed cell with two different spatial signal transduction motifs. We derived and discuss criteria

that can be used to test the well-mixed assumption and show that kinetics that connect membrane-bound species with cytosolic species naturally cause size dependence. The results are therefore of general importance for kinetic models of signal transduction.

Our findings have relevant biological implications. Since the signals transduced by linear signaling cascades from the cell membrane to the nucleus decrease exponentially on a length scale of a few microns, our theoretical findings suggest a strong cell size dependence in response to extracellular stimuli. Interesting studies of the response in cell populations often lack the response behavior attributed to cell size and morphology. Examples range from the switch-like behavior in populations of oocytes Ferrell and Machleder (1998) to the pheromone response in yeast cells Conlon et al. (2016); Banderas et al. (2016). Therefore, single cell data where the cell size is assigned to the measurements is needed for a faithful quantitative investigation of the pathway, to disentangle biochemical properties of protein-protein interactions to morphological properties such as size and shape of whole cells.

In non-linear systems, the differences that we observed in the linear signaling cascade models are likely to be amplified. Non-linear kinetics can amplify gradient formation, which leads to even stronger intracellular concentration differences Wartlick et al. (2009). This also holds for absolute concentration levels that can behave in a switch-like manner depending on the kinetics Kholodenko (2000); Ferrell and Machleder (1998). The same holds for the time scales of signaling. Higher order kinetics can amplify the accumulation time differences in different cellular locations Gordon et al. (2011).

The model can be extended to more complex spatial heterogeneities for example by using the Laplace series as suggested in this paper. With localized signals arising from membrane structures like lipid rafts, septins, co-localization due to protein-protein interactions can be represented. Since these are often precursors for cell shape and organelle structures the interplay with cell shape needs to be addressed by future research. The intrinsic geometry dependence of bulk-surface signaling systems has recently been shown for ellipsoidal cell shapes in the MinE-MinD system Halatek and Frey (2012); Thalmeier et al. (2016); Wu et al. (2016), but also in the yeast system Orlandini et al. (2013); Giese et al. (2015); Chen et al. (2016). Here, not only the global but also the local surface to volume ratio in cell protrusion plays an important role. Recent developments of mathematical methods such as the finite element method for bulk-surface equations Elliott and Ranner (2012); Eigel and Müller (2017) as well as stability analysis techniques Rubinstein et al. (2012); Edelstein-Keshet et al. (2013); Rätz and Röger (2014); Giese et al. (2015); Garcke et al. (2016); Madzvamuse et al. (2016) are expected to provide further insight in the behavior of biological systems.

METHODS

We used the finite-element software FEniCS Alnæs et al. (2015); Logg et al. (2012) to generate the corresponding meshes and to solve the arising partial differential equations in the Python programming language. The non-linear equations were solved using a fixed-point scheme Milicic et al..

AUTHOR CONTRIBUTIONS

Conceptualization, EK and WG; Methodology, EK, WG, GM and AS; Software, WG and GM; Writing – Original Draft, EK, WG and GM; Writing - Review & Editing, EK, WG, GM and AS; Supervision, EK, WG and AS; Funding Acquisition, EK and AS.

CONFLICT OF INTEREST

The authors declare no conflict of interest.

REFERENCES

Alberts, B., Johnson, A., Lewis, J., Raff, M., Roberts, K. and Walter, P. () Molecular Biology of the Cell, 5th edn, Garland Science, New York, 2007. *ISBN*, **1174808063**, 1392.

Alnæs, M. S., Blechta, J., Hake, J., Johansson, A., Kehlet, B., Logg, A., Richardson, C., Ring, J., Rognes, M. E. and Wells, G. N. (2015) The FEniCS Project Version 1.5. *Archive of Numerical Software*, **3**.

Banderas, A., Koltai, M., Anders, A. and Sourjik, V. (2016) Sensory input attenuation allows predictive sexual response in yeast. *Nature Communications*, **7**.

Beguerisse-Díaz, M., Desikan, R. and Barahona, M. (2016) Linear models of activation cascades: analytical solutions and coarse-graining of delayed signal transduction. *Journal of The Royal Society Interface*, **13**, 20160409.

Berezhkovskii, A. M., Sample, C. and Shvartsman, S. Y. (2010) How long does it take to establish a morphogen gradient? *Biophysical journal*, **99**, L59–L61.

Bhattacharyya, R. P., Reményi, A., Yeh, B. J. and Lim, W. A. (2006) Domains, motifs, and scaffolds: the role of modular interactions in the evolution and wiring of cell signaling circuits. *Annu. Rev. Biochem.*, **75**, 655–680.

Brown, G. C. and Kholodenko, B. N. (1999) Spatial gradients of cellular phospho-proteins. *FEBS letters*, **457**, 452–454.

Chay, A., Zamparo, I., Koschinski, A., Zaccolo, M. and Blackwell, K. T. (2016) Control of βAR-and N-methyl-D-aspartate (NMDA) receptor-dependent cAMP dynamics in hippocampal neurons. *PLoS Comput Biol*, **12**, e1004735.

Chen, W., Nie, Q., Yi, T.-M. and Chou, C.-S. (2016) Modelling of Yeast Mating Reveals Robustness Strategies for Cell-Cell Interactions. *PLoS computational biology*, **12**, e1004988.

Conlon, P., Gelin-Licht, R., Ganesan, A., Zhang, J. and Levchenko, A. (2016) Single-cell dynamics and variability of MAPK activity in a yeast differentiation pathway. *Proceedings of the National Academy of Sciences*, 201610081.

Diener, C., Schreiber, G., Giese, W., del Rio, G., Schröder, A. and Klipp, E. (2014) Yeast Mating and Image-Based Quantification of Spatial Pattern Formation. *PLoS Computational Biology*, **10**.

Dudin, O., Merlini, L. and Martin, S. G. (2016) Spatial focalization of pheromone/MAPK signaling triggers commitment to cell–cell fusion. *Genes & development*, **30**, 2226–2239.

Edelstein-Keshet, L., Holmes, W. R., Zajac, M. and Dutot, M. (2013) From simple to detailed models for cell polarization. *Philosophical Transactions of the Royal Society of London B: Biological Sciences*, **368**, 20130003.

Eigel, M. and Müller, R. (2017) A posteriori error control for stationary coupled bulk-surface equations. *IMA Journal of Numerical Analysis*, drw080.

Ellery, A. J., Simpson, M. J., McCue, S. W. and Baker, R. E. (2013) Simplified approach for calculating moments of action for linear reaction-diffusion equations. *Physical Review E*, **88**, 054102.

Elliott, C. M. and Ranner, T. (2012) Finite element analysis for a coupled bulk–surface partial differential equation. *IMA Journal of Numerical Analysis*, drs022.

Ferrell, J. E. and Machleder, E. M. (1998) The biochemical basis of an all-or-none cell fate switch in Xenopus oocytes. *Science*, **280**, 895–898.

Garcke, H., Kampmann, J., Rätz, A. and Röger, M. (2016) A coupled surface-Cahn–Hilliard bulk-diffusion system modeling lipid raft formation in cell membranes. *Mathematical Models and Methods in Applied Sciences*, **26**, 1149–1189.

Gelb, M. H., Brunsveld, L., Hrycyna, C. A., Michaelis, S., Tamanoi, F., Van Voorhis, W. C. and Waldmann, H. (2006) Therapeutic intervention based on protein prenylation and associated modifications. *Nature chemical biology*, **2**, 518–528.

Giese, W., Eigel, M., Westerheide, S., Engwer, C. and Klipp, E. (2015) Influence of cell shape, inhomogeneities and diffusion barriers in cell polarization models. *Physical biology*, **12**, 066014.

Gordley, R. M., Bugaj, L. J. and Lim, W. A. (2016) Modular engineering of cellular signaling proteins and networks. *Current opinion in structural biology*, **39**, 106–114.

Gordon, P. V., Sample, C., Berezhkovskii, A. M., Muratov, C. B. and Shvartsman, S. Y. (2011) Local kinetics of morphogen gradients. *Proceedings of the National Academy of Sciences*, **108**, 6157–6162.

Halatek, J. and Frey, E. (2012) Highly canalized MinD transfer and MinE sequestration explain the origin of robust MinCDE-protein dynamics. *Cell Reports*, **1**, 741–752.

Heinrich, R., Neel, B. G. and Rapoport, T. A. (2002) Mathematical models of protein kinase signal transduction. *Molecular cell*, **9**, 957–970.

Kholodenko, B., Hancock, J. and Kolch, W. (2010) Signalling ballet in space and time. *Nature reviews. Molecular cell biology*, **11**, 414—426. URL: `http://europepmc.org/abstract/MED/20495582`.

Kholodenko, B. N. (2000) Negative feedback and ultrasensitivity can bring about oscillations in the mitogen-activated protein kinase cascades. *European Journal of Biochemistry*, **267**, 1583–1588.

Klipp, E. and Liebermeister, W. (2006) Mathematical modeling of intracellular signaling pathways. *BMC neuroscience*, **7**, S10.

Klipp, E., Nordlander, B., Krüger, R., Gennemark, P. and Hohmann, S. (2005) Integrative model of the response of yeast to osmotic shock. *Nature biotechnology*, **23**, 975–982.

Klünder, B., Freisinger, T., Wedlich-Söldner, R. and Frey, E. (2013) GDI-mediated cell polarization in yeast provides precise spatial and temporal control of Cdc42 signaling. *PLoS Comput Biol*, **9**, e1003396.

Kofahl, B. and Klipp, E. (2004) Modelling the dynamics of the yeast pheromone pathway. *Yeast*, **21**, 831–850.

Levine, H. and Rappel, W.-J. (2005) Membrane-bound Turing patterns. *Physical Review E*, **72**, 061912.

Logg, A., Mardal, K.-A., Wells, G. N. et al. (2012) *Automated Solution of Differential Equations by the Finite Element Method*. Springer.

Madzvamuse, A., Ndakwo, H. S. and Barreira, R. (2016) Stability analysis of reaction-diffusion models on evolving domains: the effects of cross-diffusion. *Discrete and Continuous Dynamical Systems-Series A*, **36**, 2133–2170.

Maeder, C. I., Hink, M. A., Kinkhabwala, A., Mayr, R., Bastiaens, P. I. H. and Knop, M. (2007) Spatial regulation of Fus3 MAP kinase activity through a reaction-diffusion mechanism in yeast pheromone signalling. *Nat. Cell Biol.*, **9**, 1319–26.

Meyers, J., Craig, J. and Odde, D. J. (2006) Potential for control of signaling pathways via cell size and shape. *Current biology*, **16**, 1685–1693.

Milicic, G., Giese, W., Klipp, E. and Schröder, A. () Fixed point schemes for systems of parabolic reaction-diffusion equations. In preparation, 2017.

Muñoz-García, J., Neufeld, Z. and Kholodenko, B. N. (2009) Positional information generated by spatially distributed signaling cascades. *PLoS Comput Biol*, **5**, e1000330.

Muzzey, D., Gómez-Uribe, C. A., Mettetal, J. T. and van Oudenaarden, A. (2009) A systems-level analysis of perfect adaptation in yeast osmoregulation. *Cell*, **138**, 160–171.

Nardozzi, J. D., Lott, K. and Cingolani, G. (2010) Phosphorylation meets nuclear import: a review. *Cell Communication and Signaling*, **8**, 32.

Neves, S. R., Tsokas, P., Sarkar, A., Grace, E. A., Rangamani, P., Taubenfeld, S. M., Alberini, C. M., Schaff, J. C., Blitzer, R. D., Moraru, I. I. et al. (2008) Cell shape and negative links in regulatory motifs together control spatial information flow in signaling networks. *Cell*, **133**, 666–680.

Orlandini, E., Marenduzzo, D. and Goryachev, A. (2013) Domain formation on curved membranes: phase separation or Turing patterns? *Soft Matter*, **9**, 9311–9318.

Peletier, M. A., Westerhoff, H. V. and Kholodenko, B. N. (2003) Control of spatially heterogeneous and time-varying cellular reaction networks: a new summation law. *Journal of Theoretical biology*, **225**, 477–487.

Rätz, A. and Röger, M. (2012) Turing instabilities in a mathematical model for signaling networks. *Journal of mathematical biology*, **65**, 1215–1244.

— (2014) Symmetry breaking in a bulk–surface reaction–diffusion model for signalling networks. *Nonlinearity*, **27**, 1805.

Rubinstein, B., Slaughter, B. D. and Li, R. (2012) Weakly nonlinear analysis of symmetry breaking in cell polarity models. *Physical biology*, **9**, 045006.

Simpson, M. J., Ellery, A. J., McCue, S. W. and Baker, R. E. (2013) Critical timescales and time intervals for coupled linear processes. *The ANZIAM Journal*, **54**, 127–142.

Stelling, J. and Kholodenko, B. N. (2009) Signaling cascades as cellular devices for spatial computations. *Journal of mathematical biology*, **58**, 35–55.

Thalmeier, D., Halatek, J. and Frey, E. (2016) Geometry-induced protein pattern formation. *Proceedings of the National Academy of Sciences*, **113**, 548–553.

Thomson, T. M., Benjamin, K. R., Bush, A., Love, T., Pincus, D., Resnekov, O., Yu, R. C., Gordon, A., Colman-Lerner, A., Endy, D. and Brent, R. (2011) Scaffold number in yeast signaling system sets tradeoff between system output and dynamic range. *Proc. Natl. Acad. Sci. U.S.A.*, **108**, 20265–70.

Ventura, A. C., Bush, A., Vasen, G., Goldín, M. A., Burkinshaw, B., Bhattacharjee, N., Folch, A., Brent, R., Chernomoretz, A. and Colman-Lerner, A. (2014) Utilization of extracellular information before ligand-receptor binding reaches equilibrium expands and shifts the input dynamic range. *Proceedings of the National Academy of Sciences*, **111**, E3860–E3869.

Wang, M. and Casey, P. J. (2016) Protein prenylation: unique fats make their mark on biology. *Nature Reviews Molecular Cell Biology*, **17**, 110–122.

Wartlick, O., Kicheva, A. and Gonzalez-Gaitan, M. (2009) Morphogen gradient formation. *Cold Spring Harbor perspectives in biology*, **1**, a001255.

Wu, F., Halatek, J., Reiter, M., Kingma, E., Frey, E. and Dekker, C. (2016) Multistability and dynamic transitions of intracellular Min protein patterns. *Molecular systems biology*, **12**, 873.